Inorganic Chemistry

Communication

pubs.acs.org/IC

Fabrication of Highly Crystalline $SnNb_2O_6$ Shell with a Visible-Light Response on a $NaNbO_3$ Nanowire Core

Kenji Saito*[†,‡,§] and Akihiko Kudo[†,⊥]

[†]Department of Applied Chemistry, Faculty of Science, Tokyo University of Science, 1-3 Kagurazaka, Shinjyuku-Ku, Tokyo 162-8601, Japan

[‡]PRESTO, Japan Science and Technology Agency (JST), 4-1-8 Honcho Kawaguchi, Saitama 332-0012, Japan

[⊥]Division of Photocatalyst for Energy and Environment, Research Institute of Science and Technology, Tokyo University of Science, 1-3 Kagurazaka, Shinjuku-Ku, Tokyo 162-8601, Japan

Supporting Information

ABSTRACT: A visible-light-absorbing $SnNb_2O_6$ shell with high crystallinity was successfully fabricated on a $NaNbO_3$ nanowire through a molten salt treatment of the $NaNbO_3$ nanowire of the starting material with $SnCl_2$, whereas the fabrication was not successful on the TT phase of a niobia nanowire. The difference will come from the formation processes of $SnNb_2O_6$ crystals (ion-exchange reaction vs thermally induced crystallization reaction). The core/shell nanowire obtained from $NaNbO_3$ showed photocatalytic activity comparable to that of H_2 evolution in the presence of an electron donor under visible-light irradiation (λ > 420 nm), compared with the corresponding bulky counterpart.

Extensive efforts have been made to devise a strategy leading to structural changes in functional semiconductor materials from 3D networks to lower dimensional forms such as nanoparticle, nanowire, and nanoplate. It is important to apply these nanomaterials as potential building blocks in a variety of fields.[1−4] $SnNb_2O_6$ possesses a foordite structure in which two corner-sharing NbO_6 sheets linked together at their edges and a distorted SnO_8 sheet due to the existence of a lone-pair electron are alternating.[5] This material absorbs visible light because Sn^{II} with a $5s^2$ electronic configuration contributes to the formation of a hybrid orbital with O 2p as a valence band. So far, $SnNb_2O_6$ has been reported to function as a H_2- and O_2-evolving photocatalyst in the presence of sacrificial reagents and appropriate cocatalysts under visible-light irradiation.[6,7] The photocatalytic performance was enhanced by structural transformation from bulk to nanoplate, which was prepared by a molten $SnCl_2$ treatment of layered perovskite $Sr_2Nb_2O_7$ as a starting material.[8] Further structural changes of this material are of interest. However, a nanowire or nanoparticle structure of $SnNb_2O_6$ has yet to be reported. The molten salt treatment has been found to be effective in converting the surface of a $NaNbO_3$ nanowire ($NaNbO_3$-NW), which was obtained by the thermal reaction of a mixture of $(NH_4)_3[NbO(C_2O_4)_3]\cdot H_2O$, trioctylamine, and NaOH to visible-light-absorbing $AgNbO_3$.[9] In this context, fabrication of a $SnNb_2O_6$ shell on the $NaNbO_3$ nanowire core has merited attention.

In the present study, the molten $SnCl_2$ treatment of a $NaNbO_3$ nanowire[10] was examined, in addition to using the TT phase of a Nb_2O_5 nanowire (TT-Nb_2O_5-NW)[11] as a reference. These treated nanowires were employed as photocatalysts for H_2 and O_2 evolution reactions in the presence of sacrificial reagents under visible-light irradiation (λ > 420 nm).

Figure 1 shows XRD patterns of powders obtained after the molten $SnCl_2$ treatment of TT-Nb_2O_5-NW and $NaNbO_3$-NW.

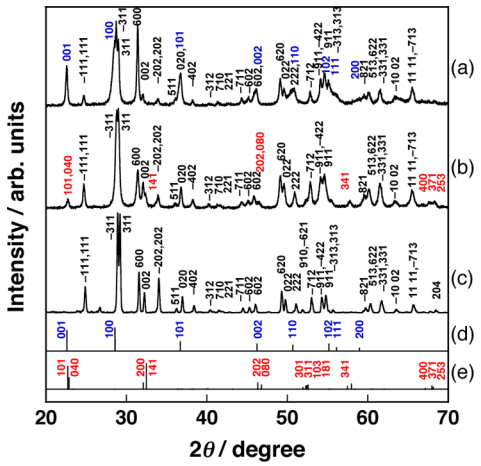

Figure 1. XRD patterns of (a) $SnNb_2O_6$/TT-Nb_2O_5-NW, (b) $SnNb_2O_6$/$NaNbO_3$-NW, (c) $SnNb_2O_6$-B, (d) TT-Nb_2O_5 (PDF 28-0317), and (e) $NaNbO_3$ (PDF 33-1270). Miller indices due to TT-Nb_2O_5 and $NaNbO_3$ are highlighted in blue and red, respectively, for clarity.

The XRD patterns indicated that obtained powders were a mixture of monoclinic $SnNb_2O_6$ [lattice constants are a = 17.063(3) Å, b = 4.8838(7) Å, and c = 5.5775(11) Å] with pseudohexagonal TT-Nb_2O_5 [lattice constants are c = 3.951(13) Å and a = 3.6158(9) Å] or monoclinic $SnNb_2O_6$ [lattice constants are a = 17.065(3) Å, b = 4.8755(10) Å, and c = 5.5781(12) Å] with orthorhombic $NaNbO_3$ [lattice constants are a = 5.5588(3) Å, b = 15.608(3) Å, and c = 5.4853(3) Å]. $NaNbO_3$-NW was converted to $SnNb_2O_6$ more efficiently than TT-Nb_2O_5-NW. (600)/(002) of $SnNb_2O_6$/TT-Nb_2O_5-NW was stronger than that of $SnNb_2O_6$-B. The crystal structure of

Received: November 7, 2012
Published: April 30, 2013

   dx.doi.org/10.1021/ic4002175 | Inorg. Chem. 2013, 52, 5621−5623

$SnNb_2O_6$ with inputting crystal plane (Figure S1) suggests that (600) has possibly causes the preferred orientation if anisotropic grain growth occurs along with *bc* plane. Half-widths of (−111) reflections of $SnNb_2O_6$ were determined in order to roughly estimate their crystallinities. The half-widths were in the order $SnNb_2O_6$-B (0.20°) < $SnNb_2O_6$/TT-Nb_2O_5-NW (0.26°) = $SnNb_2O_6$/$NaNbO_3$-NW (0.27°). To confirm which of the peak broadenings of $SnNb_2O_6$/TT-Nb_2O_5-NW and $SnNb_2O_6$/$NaNbO_3$-NW compared with that of $SnNb_2O_6$-B was due to poor crystallinity or small crystallite size, microscopic analyses by SEM and high-resolution TEM (HR-TEM) were carried out. SEM images (Figure S2) indicated that $SnNb_2O_6$/TT-Nb_2O_5-NW obtained from TT-Nb_2O_5-NW[11] possessed a structure in which grains with ca. 100 nm size were connected with each other, forming a continuous network. Short nanowires and particles coexisted near the surface of the network. $SnNb_2O_6$/TT-Nb_2O_5-NWs prepared by using 5% excess $SnCl_2$ under heat treatment at 623 K for 30 h and a 2-fold excess of $SnCl_2$ under heat treatment at 673 K for 12 h possessed nanoparticles and ca. 100-nm-thick plate morphologies, respectively. Thus, the continuous network seen in $SnNb_2O_6$/TT-Nb_2O_5-NW was created by severely limited conditions. On the other hand, nanowire morphology of $NaNbO_3$[10] was maintained for $SnNb_2O_6$/$NaNbO_3$-NW at this SEM resolution. TEM of $SnNb_2O_6$/$NaNbO_3$-NW showed evidence of a core/shell structure that appeared as areas of contrast density (Figure S2). Clear lattice fringes on the core and the widths of the fringes were estimated as 0.82 ± 0.01 nm, the value of which agreed well with (200) due to $SnNb_2O_6$ (Figure 2a and 2b). STEM-EDX

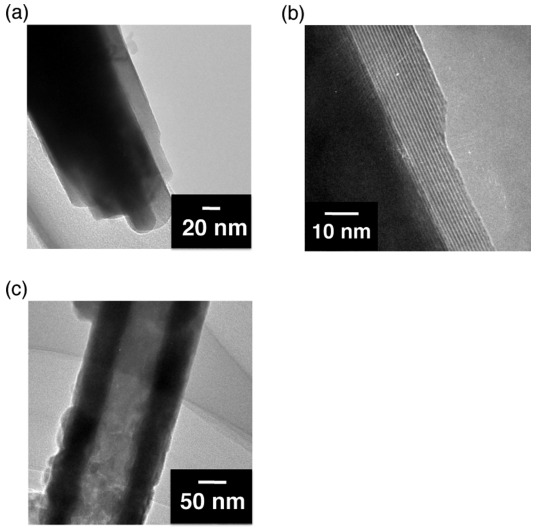

Figure 2. HR-TEM images of (a) $SnNb_2O_6$/$NaNbO_3$-NW, (b) the magnified view of part a, and (c) $SnNb_2O_6$/TT-Nb_2O_5-NW.

elemental mapping images further supported this result (Figure S3). It is difficult to distinguish the thin shell from the core because of the small sample volume of the shell. However, Nb and Na components were clearly overlapped with the blurred Sn component, suggesting a $NaNbO_3$/$SnNb_2O_6$ core/shell structure. Consistent with the TEM results, XPS indicated that $SnNb_2O_6$ existed at the surface of the nanowire because the atomic ratio of Sn/Nb was almost the same between $SnNb_2O_6$/$NaNbO_3$-NW and $SnNb_2O_6$-B (Table S1 in the SI). The composition of a single nanowire was further analyzed by TEM-EDX. $NaNbO_3$ existed at a rate of 30.9% in $SnNb_2O_6$/$NaNbO_3$-NW (Table S1 in the SI). Because the thickness of the $SnNb_2O_6$ layer was ca. 20 nm, the broadening of the (−111) diffraction peak compared with that of $SnNb_2O_6$-B will be due to the small crystallite size. Using the Scherrer equation, the crystallite size of $SnNb_2O_6$ in $SnNb_2O_6$/$NaNbO_3$-NW was determined as 17.7 ± 0.6 nm. This was consistent with the TEM result (Figure 2b). $SnNb_2O_6$/TT-Nb_2O_5-NW also had a core/shell structure judging from the contrast (Figure 2c). However, lattice fringes were not observed in this case, suggesting less crystallinity of the $SnNb_2O_6$ shell than that of $SnNb_2O_6$/$NaNbO_3$-NW. TEM-EDX results suggested that only 8.1% of $SnNb_2O_6$ existed in the $SnNb_2O_6$/TT-Nb_2O_5-NW sample. An excess amount of Nb was detected for $SnNb_2O_6$/TT-Nb_2O_5-NW by XPS compared with $SnNb_2O_6$-B. The results would originate from one of the following possibilities: (1) this sample was a mixture of $SnNb_2O_6$/TT-Nb_2O_5-NW with unreacted TT-Nb_2O_5-NW; (2) the unreacted TT-Nb_2O_5 region was partially exposed on the $SnNb_2O_6$/TT-Nb_2O_5-NW surface. These results precluded a clear estimation of the reason for XRD peak broadening. The $SnNb_2O_6$ crystallite size in $SnNb_2O_6$/TT-Nb_2O_5-NW was 41.1 ± 2.7 nm using the Scherrer equation and thereby larger than that in $SnNb_2O_6$/$NaNbO_3$-NW. The differences in the formation and crystallization of the $SnNb_2O_6$ shells $NaNbO_3$- and TT-Nb_2O_5-NW used herein will be due to the reaction processes. When TT-Nb_2O_5-NW is used, thermally induced crystallization of $SnNb_2O_6$ like a solid-state reaction on the nanowires takes place. On the other hand, $NaNbO_3$ can function as a reaction substrate for an ion-exchange reaction of Na^+ with Sn^{2+}. The latter process will be favorable to maintaining the nanowire structure. BET surface areas of $SnNb_2O_6$/TT-Nb_2O_5-NW and $SnNb_2O_6$/$NaNbO_3$-NW were 17 and 14 $m^2\ g^{-1}$, respectively. These values were more than 10 times larger than the $SnNb_2O_6$ bulk (0.9 $m^2\ g^{-1}$) but lower than the pristine nanowires (63 and 38 $m^2\ g^{-1}$ for TT-Nb_2O_5-NW and $NaNbO_3$-NW, respectively). As established by the microscopic and spectroscopic results, highly crystalline $SnNb_2O_6$ was homogeneously fabricated on $NaNbO_3$-NW. Such an increase in the crystallinity generally lowers the surface area. In contrast, the molten $SnCl_2$ treatment lowered the structural homogeneity of TT-Nb_2O_5-NW, affording a mixture of grains as a major species with short nanowires and particles. This would be the major reason for the low surface area of $SnNb_2O_6$/TT-Nb_2O_5-NW.

DRS spectra of $SnNb_2O_6$/TT-Nb_2O_5-NW and $SnNb_2O_6$/$NaNbO_3$-NW are shown in Figure S2 in the SI, in addition to nontreated TT-Nb_2O_5-NW, $NaNbO_3$-NW, and $SnNb_2O_6$-B as the references. Onset wavelengths in absorptions were red-shifted significantly by the treatment of TT-Nb_2O_5-NW and $NaNbO_3$-NW with molten $SnCl_2$. The spectral shapes indicated that $SnNb_2O_6$/TT-Nb_2O_5-NW contained a small amount of the $SnNb_2O_6$ component, in good agreement with the XRD and TEM-EDX results. $SnNb_2O_6$/$NaNbO_3$-NW contained a larger amount of $SnNb_2O_6$ than $SnNb_2O_6$/TT-Nb_2O_5-NW. The red shift in the absorptions was attributable to the contribution of the Sn $5s^2$ orbital to the formation of a hybrid orbital with O 2p as the valence band at a more negative potential than the O 2p orbital. The band gap estimated by absorption edges was 2.3 eV, identical with that of $SnNb_2O_6$-B.

Photocatalytic reactions for H_2 and O_2 evolution (Table 1) were carried out in the presence of methanol or $AgNO_3$, each of which acts as an electron donor or an acceptor, under visible-light irradiation (λ > 420 nm). Both nanowires showed almost no photoresponse regarding an O_2 evolution reaction, although highly crystalline $SnNb_2O_6$ was formed on the $NaNbO_3$

dx.doi.org/10.1021/ic4002175 | *Inorg. Chem.* 2013, 52, 5621−5623

Table 1. H_2 and O_2 Evolution Reactions over $SnNb_2O_6$-Based Photocatalysts in the Presence of Methanol and $AgNO_3$ under Visible-Light Irradiation[a]

photocatalyst	BG/eV[b]	Pt cocatalyst/wt %	rate of gas evolution/ μmol h^{-1} H_2[c]	O_2[d,e]
$SnNb_2O_6$/TT-Nb_2O_5-NW	2.3	0	0	0
$SnNb_2O_6$/TT-Nb_2O_5-NW	2.3	0.3	0.7	
$SnNb_2O_6$/TT-Nb_2O_5-NW	2.3	1.0	1.0	
TT-Nb_2O_5-NW	3.3	1.0	0	
TT-Nb_2O_5-NW	3.3	0		0
$SnNb_2O_6$/$NaNbO_3$-NW	2.3	0		t
$SnNb_2O_6$/$NaNbO_3$-NW	2.3	0.3	5.5	
$SnNb_2O_6$/$NaNbO_3$-NW	2.3	0.5	5.6	
$SnNb_2O_6$/$NaNbO_3$-NW	2.3	1.0	10	
$SnNb_2O_6$/$NaNbO_3$-NW	2.3	1.5	5.4	
$NaNbO_3$-NW	3.4	1.0	1.1	
$NaNbO_3$-NW	3.4	0		0
$SnNb_2O_6$-B	2.3	0	0	0.9
$SnNb_2O_6$-B	2.3	0.3	14	
$SnNb_2O_6$-B	2.3	0.5	12	–
$SnNb_2O_6$-B	2.3	1.0	0	–

[a]Catalyst, 0.1 g; reactant solution, 150 mL; light source, 300 W xenon-arc lamp (λ > 420 nm); cell, top-irradiation Pyrex cell. [b]BG represents the band gap. [c]10 vol % of an aqueous methanol solution. [d]0.02 mol L^{-1} of an aqueous silver nitrate solution. [e]Initial rate of O_2 evolution.

nanowire surface. However, this is in agreement with the previous reports using $SnNb_2O_6$-B.[6,7] $SnNb_2O_6$/TT-Nb_2O_5-NW showed low activity for the H_2 evolution reaction. In contrast, a $SnNb_2O_6$/$NaNbO_3$ composite nanowire showed activity comparable with that of the bulk when an optimized amount of platinum cocatalyst was loaded onto the photocatalysts. Here, the conduction band potentials of TT-Nb_2O_5-NW with a 3.3 eV band gap and of $NaNbO_3$-NW with a 3.4 eV band gap[10] will lie at −0.3 and −0.4 eV vs NHE, respectively, because the valence bands of these nanowires consist of O 2p orbitals, of which the potential is ca. 3 eV vs NHE. Taking band gaps of $SrNb_2O_6$ (3.85 eV)[12] and $SnNb_2O_6$ (2.3 eV) into account, the conduction and valence band levels of $SnNb_2O_6$ will lie at around −0.85 and 1.55 eV, respectively. Hence, photogenerated electron transfer from the $SnNb_2O_6$ shell to the TT-Nb_2O_5- or $NaNbO_3$-NW core is exothermic.[8] However, because the edge and sidewall of the TT-Nb_2O_5- or $NaNbO_3$-NW core will be covered with $SnNb_2O_6$, the conduction band electron in the TT-Nb_2O_5 or $NaNbO_3$ core is considered to make no contribution to the water reduction reaction. Thus far, efforts devoted to enhance the photocatalytic performance of the bulk under visible light by semiconductor nanowires have been hampered.[13,14] Herein, this was overcome by transcription of the $SnNb_2O_6$ crystal onto $NaNbO_3$-NW while maintaining high crystallinity, through ion exchange of Na^+ with Sn^{2+} ions. This work will offer a new strategy to developing a visible-light-responsive semiconductor nanowire possessing a superior photocatalytic performance.

In conclusion, a molten salt treatment of simple and complex niobate (TT-Nb_2O_5 and $NaNbO_3$) nanowires was examined in order to fabricate visible-light-responsive $SnNb_2O_6$ layers on the niobate nanowires. Structural characterizations using XRD, HR-TEM, and XPS indicated that the $SnNb_2O_6$ shell on the $NaNbO_3$ nanowire core possessed high crystallinity, in contrast to that on TT-Nb_2O_5-NW. The nanowire-dependent crystallization of $SnNb_2O_6$ originated from different reaction processes: thermally induced crystallization versus ion exchange. $SnNb_2O_6$/$NaNbO_3$-NW showed an activity for the H_2 evolution reaction comparable with that of the corresponding bulk in the presence of an electron donor under visible-light irradiation.

■ ASSOCIATED CONTENT

Supporting Information

Experimental section, crystal structure of $Sn_2Nb_2O_6$ with inputting (600), SEM images, STEM-EDX mapping results, summary of elemental analyses, and DRS. This material is available free of charge via the Internet at http://pubs.acs.org.

■ AUTHOR INFORMATION

Corresponding Author

*E-mail: ksaito@eng.niigata-u.ac.jp.

Present Address

[§]K.S.: Office for Development of Young Researchers, Research Planning and Promotion Division, Niigata University, 8050 Ikarashi 2-no-cho, Nishi-ku, Niigata 950-2181, Japan.

Author Contributions

The manuscript was written through the contributions of all authors. All authors have given approval to the final version of the manuscript.

Notes

The authors declare no competing financial interest.

■ ACKNOWLEDGMENTS

This work was financially supported by the PRESTO (Precursory Research for Embryonic Science and Technology) project.

■ REFERENCES

(1) Reiss, P.; Protiére, M.; Li, L. *Small* **2009**, *5*, 154.
(2) Guo, S.; Wang, E. *Acc. Chem. Res.* **2011**, *44*, 491.
(3) Huang, M. H.; Lin, P.-H. *Adv. Funct. Mater.* **2012**, *22*, 14.
(4) Joshi, R. K.; Schneider, J. J. *Chem. Soc. Rev.* **2012**, *41*, 5285.
(5) Cruz, L. P.; Savariault, J.-M.; Rocha, J.; Jumas, J.-C.; Pedrosa de Jesus, J. D. *J. Solid State Chem.* **2001**, *156*, 349.
(6) Hosogi, Y.; Tanabe, K.; Kato, H.; Kobayashi, H.; Kudo, A. *Chem. Lett.* **2004**, *33*, 28.
(7) Hosogi, Y.; Shimodaira, Y.; Kato, H.; Kobayashi, H.; Kudo, A. *Chem. Mater.* **2008**, *20*, 1299.
(8) Hosogi, Y.; Kato, H.; Kudo, A. *Chem. Lett.* **2006**, *35*, 578.
(9) Saito, K.; Koga, K.; Kudo, A. *Nanosci. Nanotechnol. Lett.* **2011**, *3*, 686.
(10) Saito, K.; Kudo, A. *Inorg. Chem.* **2010**, *49*, 2017.
(11) Saito, K.; Kudo, A. *Bull. Chem. Soc. Jpn.* **2009**, *82*, 1030.
(12) Cho, I.-S.; Bae, S. T.; Kim, D. H.; Hong, K. S. *Int. J. Hydrogen Energy* **2010**, *35*, 12954.
(13) Bao, N.; Shen, L.; Takata, T.; Lu, D.; Domen, K. *Chem. Lett.* **2006**, *35*, 318.
(14) Yu, J.; Kudo, A. *Adv. Funct. Mater.* **2006**, *16*, 2163.

dx.doi.org/10.1021/ic4002175 | *Inorg. Chem.* 2013, 52, 5621−5623